







## Rydberg series of dark excitons and the conduction band spin-orbit splitting in monolayer WSe<sub>2</sub>

Piotr Kapuściński <sup>1,2</sup>, Alex Delhomme<sup>1</sup>, Diana Vaclavkova<sup>1</sup>, Artur O. Slobodeniuk<sup>3</sup>, Magdalena Grzeszczyk <sup>4</sup>, Miroslav Bartos<sup>5</sup>, Kenji Watanabe <sup>6</sup>, Takashi Taniguchi <sup>7</sup>, Clément Faugeras <sup>1</sup> & Marek Potemski <sup>1,4</sup>✉

Strong Coulomb correlations together with multi-valley electronic bands in the presence of spin-orbit interaction are at the heart of studies of the rich physics of excitons in monolayers of transition metal dichalcogenides (TMD). Those archetypes of two-dimensional systems promise a design of new optoelectronic devices. In intrinsic TMD monolayers the basic, intravalley excitons, are formed by a hole from the top of the valence band and an electron either from the lower or upper spin-orbit-split conduction band subbands: one of these excitons is optically active, the second one is dark, although possibly observed under special conditions. Here we demonstrate the s-series of Rydberg dark exciton states in tungsten diselenide monolayer, which appears in addition to a conventional bright exciton series in photoluminescence spectra measured in high in-plane magnetic fields. The comparison of energy ladders of bright and dark Rydberg excitons is shown to be a method to experimentally evaluate one of the missing band parameters in TMD monolayers: the amplitude of the spin-orbit splitting of the conduction band.

<sup>1</sup>LNCMI-EMFL, CNRS UPR3228, Univ. Grenoble Alpes, Univ. Toulouse, Univ. Toulouse 3, INSA-T, Grenoble and Toulouse, France. <sup>2</sup>Department of Experimental Physics, Wrocław University of Technology, Wrocław, Poland. <sup>3</sup>Department of Condensed Matter Physics, Faculty of Mathematics and Physics, Charles University, Praha, Czech Republic. <sup>4</sup>Institute of Experimental Physics, Faculty of Physics, University of Warsaw, Warszawa, Poland. <sup>5</sup>Central European Institute of Technology, Brno University of Technology, Brno, Czech Republic. <sup>6</sup>Research Center for Functional Materials, National Institute for Materials Science, Tsukuba, Japan. <sup>7</sup>International Center for Materials Nanoarchitectonics, National Institute for Materials Science, Tsukuba, Japan. ✉email: [marek.potemski@lncmi.cnrs.fr](mailto:marek.potemski@lncmi.cnrs.fr)

In most of low-dimensional, direct-gap semiconductor systems (quantum wells and monolayers of transition metal dichalcogenides, quantum wires, and dots), the near band edge electron-hole excitations, the excitonic states, can be classified into two categories depending whether their associated projection of the total angular momentum is  $j_z = \pm 1$  or it is  $j_z = \pm 2$  or 0. According to standard selection rules for optical transitions, the excitons with  $j_z = \pm 1$  can be excited by light and/or can recombine by emitting photons and are therefore referred to as bright excitons. Instead, excitons with  $j_z = \pm 2$  or 0 are termed dark as they do not efficiently couple to the radiation field. Although dark, the  $j_z = \pm 2$  or  $j_z = 0$  excitons can be brightened under special conditions, e.g., under application of the magnetic field in an appropriate configuration<sup>1,2</sup> and thus possibly initiating the photoluminescence signal (though still hardly observed in absorption-type spectra). Dark excitons can largely alter the dynamics of optical excitations and, as long-lived bosonic quasiparticles, are possible candidates to form a condensate exciton phase<sup>3</sup>. Those states have been the object of vast investigations in semiconductor quantum wells, dots, and wires, in carbon nanotubes and more recently in monolayer semiconductors<sup>4–19</sup>. All these studies have been however largely focused on excitonic ground states, whereas the physics of dark excitons associated with the excited excitonic states is a little-explored area<sup>20–22</sup>. This, in particular, applies to two-dimensional semiconductors which often display a characteristic series of Rydberg  $ns$  states of bright excitons<sup>23–26</sup>, whereas a demonstration of the corresponding series of dark excitonic states is missing so far.

In this paper, we report on low-temperature magneto-optical study of Rydberg series of excitonic states as they appear in a WSe<sub>2</sub> monolayer. Notably, in this representative example of a 2D semiconductor, the rich spectrum of excited excitonic states can be relatively easily traced with luminescence experiments<sup>25,27–29</sup>. Profiting on this fact, we brighten dark excitons in our sample by applying an in-plane magnetic field and uncover their  $ns$  ( $n = 1$ , up to 4) Rydberg series which appears in addition to a Rydberg spectrum of bright excitons<sup>24,25</sup>. By comparing energy diagrams of dark and bright exciton series, we experimentally derive the single-particle separation between spin-orbit-split conduction band subbands in a WSe<sub>2</sub> monolayer. Intriguingly, this separation is found to be of about two times smaller than that commonly assumed from theoretical modeling of electronic bands of monolayer semiconductors.

## Results and discussion

The focus of our study can be clearly read from Fig. 1. Figure 1a illustrates a simple generic scheme of the band structure of a WSe<sub>2</sub> monolayer, as it is found in a close vicinity of the direct bandgap at the two  $K^+$  and  $K^-$  points of the Brillouin zone. We consider only three relevant bands (per each  $K^+$  and  $K^-$  point): two spin-orbit split subbands in the conduction band (weakly separated in energy, by  $\Delta_c \approx$  tens of meVs) but only one, top valence subband (neglecting the lower one separated by hundreds of meVs from the upper subband). As generally accepted and shown in Fig. 1a, the interband, intravalley transitions which involve the electronic states of the upper conduction subband are optically allowed, whereas those associated with the lower subband are characterized by  $j_z = 0$  and thus are not optically active under conventional conditions/configurations<sup>7,30</sup>. The  $j_z = 0$  transitions are weakly allowed only in the configuration for which the electromagnetic wave has its  $k$ -vector aligned along the monolayer plane and nonzero out of plane component of the electric field, or in the presence of an in-plane magnetic field. Please, note, that in the case of TMD monolayers, the  $j_z = \pm 1$  selection rules for optical transitions coincide with the ansatz of conservation of electronic spins in optical transitions. The band-to-band image of optical transitions is not, however, sufficient to describe the optical response of semiconductors, and in particular that of the investigated structure: the electron-hole Coulomb interaction and hence the excitonic effects have to be taken into account. As shown in Fig. 1b, one may expect the appearance of two distinct  $ns$  Rydberg series of near band edge excitons in our WSe<sub>2</sub> monolayer: the routinely observed bright exciton series<sup>23–26</sup> associated with the upper conduction band subband, but also the dark-exciton series associated with the lower conduction band subband, revealed in the present report. In the limit of large  $n$ , the energy difference between bright and dark-exciton states provides a measure of the spin-orbit splitting of the conduction band  $\Delta_c = E_g^B - E_g^D$ , where  $E_g^B$  and  $E_g^D$  denote, correspondingly, the single-particle bandgaps associated with upper and lower conduction band subbands. It is worth noting, that the energy difference  $\Delta_{DB}$  between the ground states of dark and bright excitons depends also on their respective,  $E_b^D$  and  $E_b^B$ , binding energies:  $\Delta_{DB} = \Delta_c + (E_b^D - E_b^B)$ . Since  $E_b^D$  and  $E_b^B$  are a priori different, measuring the  $\Delta_{DB}$  parameter alone does not infer the amplitude of  $\Delta_c$ .

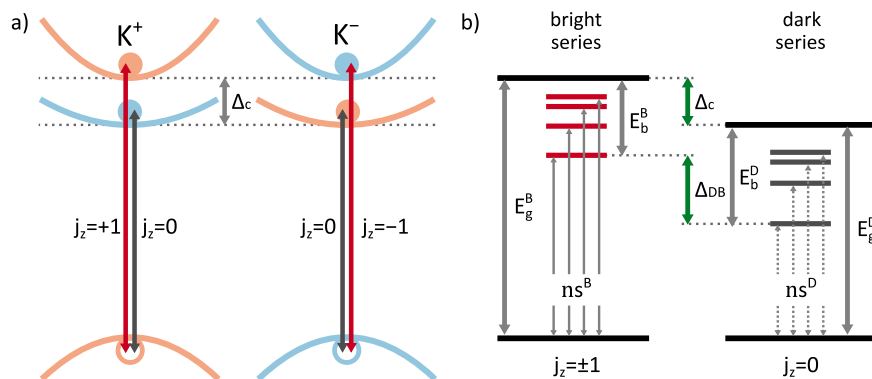


**Fig. 1 Schematic illustrations of bright and dark transitions in WSe<sub>2</sub> monolayer.** **a** Schematic representation of the interband transitions in a single-particle picture. The spin-up and spin-down states are shown as light-orange and light-blue parabolas, respectively. Optically active (bright) transitions at  $K^+$  and  $K^-$  valleys are represented by the red arrows, while optically inactive (dark) transitions are depicted in dark gray. The light-gray arrow represents the conduction band spin-orbit splitting ( $\Delta_c$ ). **b** The energy diagram of excitonic transitions: Rydberg series of bright ( $ns^B$ ) and dark ( $ns^D$ ) resonances. The horizontal red and dark-gray lines represent bright and dark excitonic levels, respectively. The light-gray arrows represent the bandgaps for bright and dark excitons ( $E_g^{B/D}$ ) and the binding energies of the ground states of bright and dark excitons ( $E_b^{B/D}$ ). The energy splitting between ground states of bright and dark excitons ( $\Delta_{DB}$ ) and the conduction band spin-orbit splitting ( $\Delta_c$ ) are represented by the green arrows.

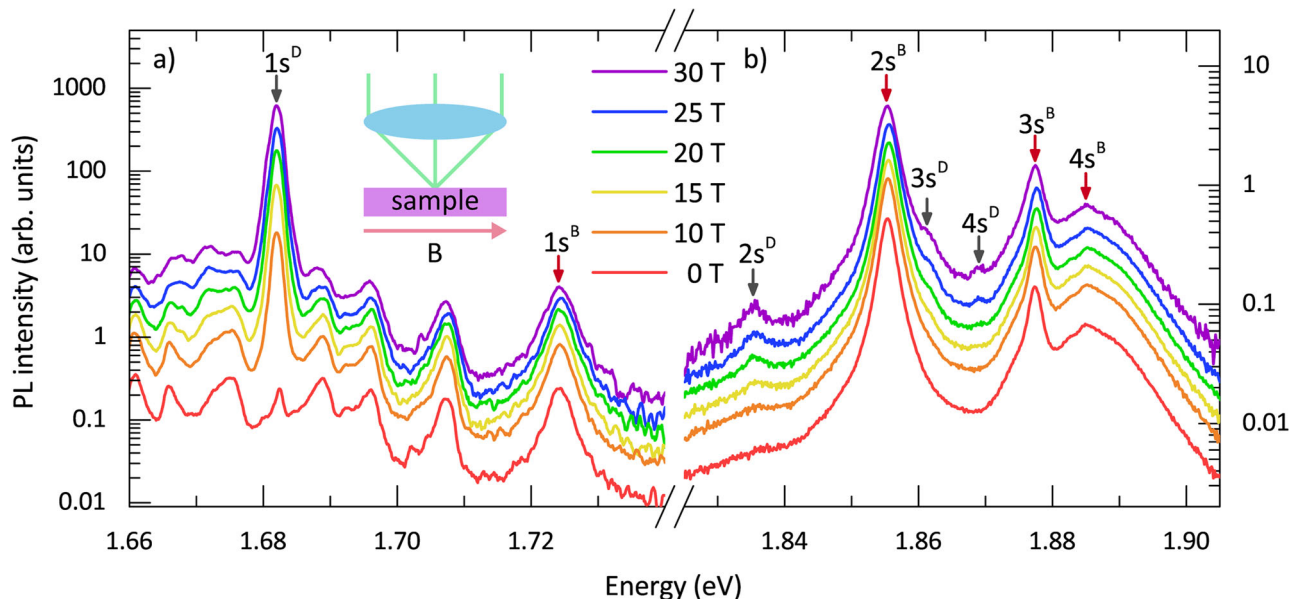


**Fig. 2 Magnetic field-dependence of emissions from bright and dark-exciton Rydberg states.** Low-temperature photoluminescence (PL) spectra in arbitrary (arb.) units measured at selected in-plane magnetic fields in the energy region of both **a** ground and **b** excited states. Spectra were shifted for clarity and normalized to the  $1s^B$  feature in the lower energy region and to the  $2s^B$  feature in the higher-energy region. Note that the intensity scales differ for these two regions. The inset schematically shows the backscattering geometry used in the experiment, where the excitation and the collected light beams are quasi-perpendicular to the sample surface.

The active part of the structure used for the experiments is a  $WSe_2$  monolayer extracted from a commercially available tungsten diselenide crystal. The monolayer was encapsulated in between hexagonal boron nitride (hBN) flakes and deposited on a Si substrate, following the conventional methods of mechanical exfoliation and deterministic dry transfer techniques. Experiments consisted of low-temperature (4.2 K) magnetophotoluminescence measurements carried out in magnetic fields up to 30 T, applied along the monolayer plane. As sketched in the inset to Fig. 2, we used the backscattering geometry where both the excitation and the collected light beams were quasi-perpendicular to the sample/monolayer. More details on sample preparation and experimental details can be found in the “Methods” section.

Representative photoluminescence spectra of the investigated  $WSe_2$  monolayer are presented in Fig. 2. Inspecting the low spectral range (Fig. 2a), one recognizes a characteristic set of multiple photoluminescence transitions, typical of  $WSe_2$  monolayers<sup>31–33</sup>. Possible formations of many different excitonic states (including nontrivial indirect/inter-valley excitons and excitonic complexes such as trions and biexcitons) account for the spectrum complexity which we disregard here, focusing our attention on neutral, bright, and dark intravalley excitons. First, we examine the photoluminescence (PL) spectrum measured in the absence of magnetic field ( $B$ ), and, in accordance to previous reports<sup>24,25,27–29</sup>, recognize the characteristic sequence of emission peaks related to the Rydberg series of  $1s^B$ ,  $2s^B$ ,  $3s^B$ , up to  $4s^B$  states of bright excitons. The PL spectrum measured at  $B=0$  shows also a weak transition related to the ground state,  $1s^D$ , of dark exciton<sup>6–8</sup>. Note that no additional emission features can be found between  $1s^B$  and  $2s^B$  states (see Supplementary Fig. S3). This is because this low energy state is largely populated (under optical excitation) and because the emission from this state is legitimate in the direction along the monolayer plane, thus weakly visible in our spectrum collected using the objective with a relatively large numerical aperture<sup>7,8</sup>. Please note, that we employ here a simplified picture of the dark exciton and view it as raising

only a single resonance, i.e., we ignore its doublet, dark-gray components split by  $\approx 0.7$  meV<sup>6,8</sup>, the energy which is negligibly small in the context of our further considerations.

Central for our report is the study of the evolution of the PL spectra measured as a function of the in-plane magnetic field ( $B_{\parallel}$ ). Such studies have been already successfully applied to unveil the ground ( $1s^D$ ) states of dark excitons in most of TMD monolayers<sup>8–11,34</sup>. The application of the in-plane magnetic field induces the Zeeman effect, and thus the mixing of spin-orbit split conduction subbands; dark excitons acquire an oscillator strength ( $\sim B_{\parallel}^2$ ) for the emission in the direction perpendicular to the monolayer plane and become apparent in the PL spectra. The efficient magnetic brightening of the ground state of the dark exciton in  $WSe_2$  monolayer is confirmed by the present experiments. As can be seen in Fig. 2a, the intensity of the  $1s^D$  emission grows progressively as a function of  $B_{\parallel}$ , and eventually dominates the PL spectrum in the limit of high magnetic fields. Importantly, new transitions driven by the application of the in-plane magnetic field appear also in the higher spectral range (see Fig. 2b) in the vicinity of the PL peaks associated to the excited states of bright excitons. These new transitions, labeled as  $2s^D$ ,  $3s^D$ , and  $4s^D$  in Fig. 2, are attributed to the excited Rydberg states of the dark exciton.

As demonstrated in Fig. 3, the magnetic brightening of dark-exciton states, i.e., the increase of the relative intensity  $I_D(n)/I_B(n)$  of dark  $ns^D$  emission peak with respect to its bright  $ns^B$  counterpart, roughly follows the expected  $I_D(n)/I_B(n) = b_n B_{\parallel}^2$  rule (see Supplementary Note 1 and Supplementary Figs. S1 and S2 for more details on data analysis and estimation of the PL intensities). This, however, is not true in the case of ground states for the in-plane fields  $B_{\parallel} > 20$  T, where the relative intensity deviates from the quadratic dependence, possibly due to the shortened (by optical activation) dark-exciton lifetime leading to the decrease of the dark-exciton population. Hence, only the datapoints for  $B_{\parallel} < 20$  T were used for the estimation of  $b_1$ . The  $b_n$  coefficients reflect the relative oscillator strength  $r_n = r_{ns}^D/r_{ns}^B$  as well as the relative population  $p_n = N_{ns}^D/N_{ns}^B$  (under optical

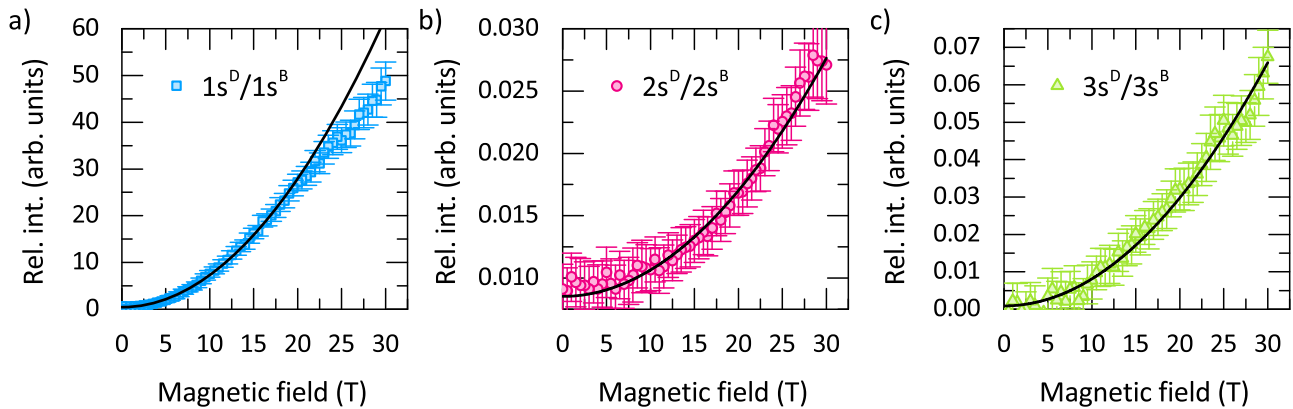


**Fig. 3 Brightening of the dark-exciton Rydberg states.** Intensities of dark states relative to the intensity of bright states (Rel. int. =  $I_D(n)/I_B(n)$ ) as a function of the in-plane magnetic field for **a** the 1s states (blue squares), **b** the 2s states (red circles), and **c** the 3s states (green triangles) along with quadratic fits (black lines) of the form  $a + bx^2$ . Note that in the case of 1s states, only datapoints from 0 T to 20 T were considered for the fitting, as for higher fields, the relative intensity clearly starts to deviate from quadratic dependence. The error bars represent combined standard uncertainties resulting from the uncertainties of the estimation of the photoluminescence intensities of bright and dark-exciton states. More details on this estimation can be found in Supplementary Note 1.

excitation) of corresponding dark  $ns^D$  and bright  $ns^B$  states:  $b_n = r_n \cdot p_n$ . Comparing the extracted  $b_n$  parameters with theoretically expected values for  $r_n$  (see Supplementary Note 2), we find that dark and bright states are not far from being equally populated for pairs of the excited states ( $p_n \approx 2$  for  $n = 2, 3$ ). On the other hand, the population of the ground dark state ( $1s^D$ ) is estimated to be five orders of magnitude higher than that of the  $1s^B$  ground bright state ( $p_n \approx 10^5$ ). As discussed in more detail in Supplementary Note 2, the population of excitonic states under optical transitions in WSe<sub>2</sub> monolayers appears to be highly nonthermal, which needs its explanation with a future comprehensive study of PL dynamics in these systems.

Energy diagrams of both dark and bright exciton series are of particular interest. Central positions of  $1s^D$  and  $1s^B$  emission peaks (at  $E_{1s}^D = 1.682$  eV and  $E_{1s}^B = 1.725$  eV, respectively) can be directly read from the measured spectra with reasonable precision, whereas the central energies of transitions associated with excited excitonic states have been extracted by reproducing the high energy part of the spectra with multiple Lorentzian resonances (see Supplementary Fig. S2 and Supplementary Table S1). As shown in Fig. 4, both series of bright and dark excitonic resonances follow the previously evoked (for bright states) semi-empirical formula<sup>25</sup>:

$$E_n^{D/B} = E_g^{D/B} - \frac{Ry^{D/B}}{(n + \delta)^2}, \quad (1)$$

where  $E_g^{D/B}$  is the dark/bright bandgap associated to the lower/upper conduction band subband and,  $Ry^{D/B}$  should be, in the first approximation, identified with the effective Rydberg energy for the dark/bright exciton;  $Ry^{D/B} = 13.6 \text{ eV} \cdot \mu^{D/B} / (\epsilon^2 m_0)$ , where  $\mu^{D/B}$  is the reduced effective mass embracing the valence band hole and electron from upper/lower conduction subbands,  $\epsilon$  is the dielectric constant of the surrounding hBN material and  $m_0$  stands for the electron mass.  $\delta$  parameter, which accounts for the 2D screening length and the hBN-dielectric screening, is found to be  $\delta = -0.09$ , which is notably common for dark and bright series and well matches the previously reported value ( $-0.08$  for the bright exciton series<sup>25</sup>). The validity of the above simple formula to account for the energy ladder of 2D excitonic states in TMD monolayers encapsulated in hBN has been largely justified in ref. <sup>25</sup>, and, in particular, shown to be equivalent to the optional approach employing the Rytova–Keldysh potential<sup>24,27</sup>. As extrapolated from plots shown in Fig. 4, the extracted values of

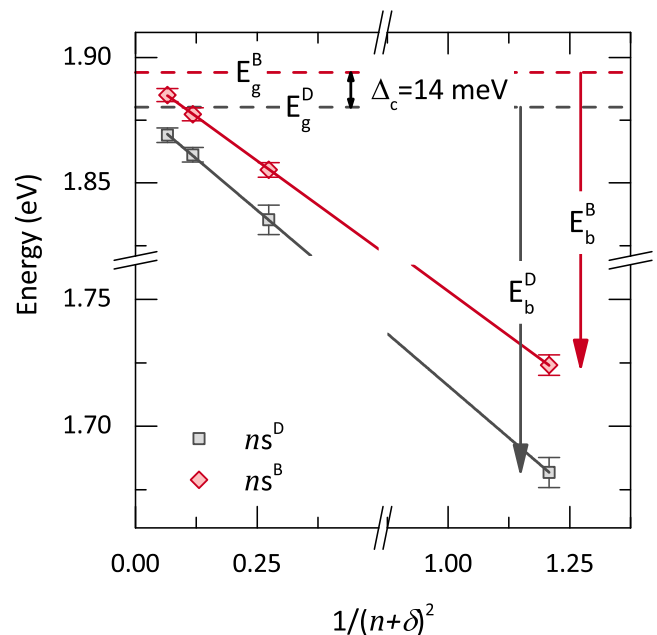


**Fig. 4 Dark and bright excitonic Rydberg series.** Experimentally obtained transition energies for the bright (red diamonds,  $ns^B$ ) and dark (gray squares,  $ns^D$ ) exciton s-series as a function of  $1/(n + \delta)^2$ , where  $\delta = -0.09$ . The error bars represent the line widths of the observed emission lines. The solid red and gray lines represent fits to the data with the model described in the text. The dashed red and gray lines denote the bandgaps for dark ( $E_g^D = 1.880$  eV) and bright ( $E_g^B = 1.894$  eV) excitons, while the red and gray arrows show the binding energies of bright ( $E_b^B = 171$  meV) and dark ( $E_b^D = 198$  meV) excitons, respectively. The conduction band splitting ( $\Delta_c = 14$  meV) is also indicated.

dark and bright bandgaps are, correspondingly,  $E_g^D = 1.8802 \pm 0.0004$  eV and  $E_g^B = 1.8940 \pm 0.0006$  eV and we eventually come up with disclosing the amplitude of the conduction band spin-orbit splitting:  $\Delta_c = E_g^B - E_g^D = 14 \pm 1$  meV. Notably, this value is to be accounted by theoretical modeling of electronic bands of TMD monolayers<sup>35–37</sup> which, as yet, overestimates it by a factor of two and a half. It is, however, important to note that the theoretical estimate<sup>35–37</sup> of  $\Delta_c \cong 36$  meV, refers to



freestanding WSe<sub>2</sub> monolayers, whereas,  $\Delta_c = 14$  meV we report, is, strictly speaking, derived for the case of WSe<sub>2</sub> monolayer embedded in hBN. The dielectric screening which is well evidenced to affect the excitonic resonances in encapsulated TMD monolayers, leads also to the renormalization of, single-particle bandgaps<sup>38,39</sup>. It remains to be clarified with advanced theoretical calculations whether the dielectric screening may differently renormalize our dark and bright bandgaps and whether the value  $\Delta_c = 14$  meV we report here applies also to other structures of WSe<sub>2</sub> monolayers.

Binding energies of bright and dark excitons:  $E_b^B = 170.6 \pm 0.4$  meV and  $E_b^D = 198.4 \pm 0.8$  meV, respectively, are two other extracted parameters. Following up our analysis (see Eq. (1) and Fig. 4), the resulting energy ratio  $\rho_{DB} = E_b^D/E_b^B = 1.16$  (or difference  $E_b^D - E_b^B = 28$  meV) is anticipated to be explained by different, for bright and dark excitons, reduced effective masses ( $E_b^D/E_b^B = \mu^D/\mu^B$ ). Indeed, when assuming the theoretically calculated masses of a valence hole ( $m_h = 0.36$ ) and electrons in two conduction subbands ( $m_e^D = 0.40$  and  $m_e^B = 0.29$ )<sup>37</sup>, we find  $\mu^D/\mu^B = 1.18$ , a value which is very close to the experimentally derived ratio  $E_b^D/E_b^B = 1.16$ . On the other hand, one may expect that the difference between  $E_b^D$  and  $E_b^B$  arises not only from the direct Coulomb term but also from the exchange term, as bright and dark excitons consist of parallel or antiparallel spin configurations, respectively<sup>40–42</sup>. Whereas we suggest here that the exchange term might be relatively small, this claim has to be taken with caution, since our estimations refer to theoretically calculated effective masses which perhaps are not sufficiently accurate. Notably, the amplitude of the exchange term, as large as 20 meV, has been theoretically predicted<sup>40</sup> but for the case of freestanding WSe<sub>2</sub> monolayers. Coulomb interaction, being effectively at the origin of the exchange term, is screened in encapsulated monolayers. With very rough estimation one would expect the reduction of the exchange term down to  $20 \text{ meV}/4.5 = 4.4$  meV in our monolayer encapsulated in hBN with dielectric constant  $\epsilon = 4.5$ . Nonetheless, our findings once again raise a question about the importance of the exchange interaction for the energy difference between the bright and dark excitons binding energies in TMD monolayers.

**Conclusions.** In this report, we demonstrated the magnetic brightening of the Rydberg *ns*-series of dark excitons, up to  $n = 4$ , in a WSe<sub>2</sub> monolayer encapsulated in hBN. The analysis of the bright and dark excitons series allowed us to determine one of the missing band parameters, the amplitude of the spin-orbit splitting in the conduction band of this broadly investigated 2D structure. Its derived value,  $\Delta_c = 14$  meV, is significantly lower than that commonly assumed, what calls for revision of theoretical calculations of electronic bands in TMD monolayers. Moreover, our results suggest that the difference between the binding energies of bright and dark excitons can be fully explained by the difference in the masses of electrons in the two spin-orbit-split conduction bands, without referring to exchange interactions.

## Methods

**Sample fabrication.** The sample used in our study is composed of WSe<sub>2</sub> monolayer encapsulated in hBN flakes and deposited on a Si substrate. The heterostructure was fabricated using mechanical exfoliation of bulk WSe<sub>2</sub> and hBN crystals. The bottom hBN layer was created by nondeterministic exfoliation onto Si substrate, while the WSe<sub>2</sub> monolayer and capping hBN flake were transferred using dry stamping technique onto the bottom hBN flake using PDMS stamps.

**Experimental setup.** The low-temperature magneto-photoluminescence experiments were performed in the Voigt configuration, with the magnetic field applied parallel to the monolayer plane using a free-beam insert placed in a resistive solenoid producing magnetic fields up to 30 T. The sample was placed on top of the *x*-*y*-*z* piezo stage and kept in gaseous helium at  $T = 4.2$  K. Continuous wave and

unpolarized excitation of 515 nm wavelength was used, with the excitation power of 200  $\mu$ W. The excitation beam was focused and the signal was collected by the same microscope objective with a numerical aperture of  $NA = 0.35$ . The unpolarized collected light was analyzed by a 0.5-m-long monochromator equipped with a 500 lines/mm grating and CCD camera.

## Data availability

The data that support the findings of this study are available from the corresponding author upon request.

Received: 22 February 2021; Accepted: 19 July 2021;

Published online: 19 August 2021

## References

- Bayer, M. et al. Fine structure of neutral and charged excitons in self-assembled In(Ga)As/(Al)GaAs quantum dots. *Phys. Rev. B* **65**, 195315 (2002).
- Slobodeniuk, A. O. & Basko, D. M. Spin-flip processes and radiative decay of dark intravalley excitons in transition metal dichalcogenide monolayers. *2D Mater.* **3**, 35009 (2016).
- Combescot, M., Combescot, R. & Dubin, F. Bose-Einstein condensation and indirect excitons: a review. *Rep. Prog. Phys.* **80**, 66501 (2017).
- Glasberg, S., Shtrikman, H., Bar-Joseph, I. & Klipstein, P. C. Exciton exchange splitting in wide GaAs quantum wells. *Phys. Rev. B* **60**, R16295–R16298 (1999).
- Bayer, M., Stern, O., Kuther, A. & Forchel, A. Spectroscopic study of dark excitons in InxGa1-xAs self-assembled quantum dots by a magnetic-field-induced symmetry breaking. *Phys. Rev. B* **61**, 7273–7276 (2000).
- Robert, C. et al. Fine structure and lifetime of dark excitons in transition metal dichalcogenide monolayers. *Phys. Rev. B* **96**, 1–8 (2017).
- Wang, G. et al. In-plane propagation of light in transition metal dichalcogenide monolayers: optical selection rules. *Phys. Rev. Lett.* **119**, 1–7 (2017).
- Molas, M. R. et al. Probing and manipulating valley coherence of dark excitons in monolayer WSe<sub>2</sub>. *Phys. Rev. Lett.* **123**, 96803 (2019).
- Lu, Z. et al. Magnetic field mixing and splitting of bright and dark excitons in monolayer MoSe<sub>2</sub>. *2D Mater.* **7**, 15017 (2019).
- Robert, C. et al. Measurement of the spin-forbidden dark excitons in MoS<sub>2</sub> and MoSe<sub>2</sub> monolayers. *Nat. Commun.* **11**, 4037 (2020).
- Zinkiewicz, M. et al. Neutral and charged dark excitons in monolayer WS<sub>2</sub>. *Nanoscale* **12**, 18153–18159 (2020).
- Kowalik, K. et al. Manipulating the exciton fine structure of single CdTe/ZnTe quantum dots by an in-plane magnetic field. *Phys. Rev. B* **75**, 195340 (2007).
- Zaric, S. et al. Optical signatures of the aharonov-bohm phase in single-walled carbon nanotubes. *Science* **304**, 1129–1131 (2004).
- Shaver, J. et al. Magnetic brightening of carbon nanotube photoluminescence through symmetry breaking. *Nano Lett.* **7**, 1851–1855 (2007).
- Srivastava, A., Htoon, H., Klimov, V. I. & Kono, J. Direct observation of dark excitons in individual carbon nanotubes: inhomogeneity in the exchange splitting. *Phys. Rev. Lett.* **101**, 87402 (2008).
- Goryca, M. et al. Brightening of dark excitons in a single CdTe quantum dot containing a single Mn<sup>2+</sup> ion. *Phys. Rev. B* **82**, 165323 (2010).
- Alexander-Webber, J. A. et al. Hyperspectral imaging of exciton photoluminescence in individual carbon nanotubes controlled by high magnetic fields. *Nano Lett.* **14**, 5194–5200 (2014).
- Zhou, Y. et al. Probing dark excitons in atomically thin semiconductors via near-field coupling to surface plasmon polaritons. *Nat. Nanotechnol.* **12**, 856–860 (2017).
- Zhang, X.-X. et al. Magnetic brightening and control of dark excitons in monolayer WSe<sub>2</sub>. *Nat. Nanotechnol.* **12**, 883–888 (2017).
- Farenbruch, A., Fröhlich, D., Yakovlev, D. R. & Bayer, M. Rydberg series of dark excitons in Cu<sub>2</sub>O. *Phys. Rev. Lett.* **125**, 207402 (2020).
- Watanabe, K., Uchida, K. & Miura, N. Magneto-optical effects observed for GaSe in megagauss magnetic fields. *Phys. Rev. B* **68**, 155312 (2003).
- Nagamune, Y., Takeyama, S. & Miura, N. Exciton spectra and anisotropic Zeeman effect in PbI<sub>2</sub> at high magnetic fields up to 40 T. *Phys. Rev. B* **43**, 12401–12405 (1991).
- Chernikov, A. et al. Exciton binding energy and nonhydrogenic Rydberg series in monolayer WS<sub>2</sub>. *Phys. Rev. Lett.* **113**, 076802 (2014).
- Stier, A. V. et al. Magneto-optics of exciton rydberg states in a monolayer semiconductor. *Phys. Rev. Lett.* **120**, 57405 (2018).
- Molas, M. R. et al. Energy spectrum of two-dimensional excitons in a nonuniform dielectric medium. *Phys. Rev. Lett.* **123**, 136801 (2019).
- Goryca, M. et al. Revealing exciton masses and dielectric properties of monolayer semiconductors with high magnetic fields. *Nat. Commun.* **10**, 4172 (2019).

27. Liu, E. et al. Magnetophotoluminescence of exciton Rydberg states in monolayer  $\text{WSe}_2$ . *Phys. Rev. B* **99**, 205420 (2019).
28. Chen, S.-Y. et al. Luminescent emission of excited Rydberg excitons from monolayer  $\text{WSe}_2$ . *Nano Lett.* **19**, 2464–2471 (2019).
29. Delhomme, A. et al. Magneto-spectroscopy of exciton Rydberg states in a CVD grown  $\text{WSe}_2$  monolayer. *Appl. Phys. Lett.* **114**, 232104 (2019).
30. Delhomme, A. et al. Flipping exciton angular momentum with chiral phonons in  $\text{MoSe}_2/\text{WSe}_2$  heterobilayers. *2D Mater.* **7**, 41002 (2020).
31. Li, Z. et al. Emerging photoluminescence from the dark-exciton phonon replica in monolayer  $\text{WSe}_2$ . *Nat. Commun.* **10**, 2469 (2019).
32. Liu, E. et al. Valley-selective chiral phonon replicas of dark excitons and trions in monolayer  $\text{WSe}_2$ . *Phys. Rev. Res.* **1**, 32007 (2019).
33. He, M. et al. Valley phonons and exciton complexes in a monolayer semiconductor. *Nat. Commun.* **11**, 618 (2020).
34. Molas, M. R. et al. Brightening of dark excitons in monolayers of semiconducting transition metal dichalcogenides. *2D Mater.* **4**, 21003 (2017).
35. Komider, K., González, J. W. & Fernández-Rossier, J. Large spin splitting in the conduction band of transition metal dichalcogenide monolayers. *Phys. Rev. B - Condens. Matter Mater. Phys.* **88**, 1–7 (2013).
36. Liu, G. Bin, Shan, W. Y., Yao, Y., Yao, W. & Xiao, D. Three-band tight-binding model for monolayers of group-VIB transition metal dichalcogenides. *Phys. Rev. B - Condens. Matter Mater. Phys.* **88**, 085433 (2013).
37. Kormányos, A. et al. kp theory for two-dimensional transition metal dichalcogenide semiconductors. *2D Mater.* **2**, 22001 (2015).
38. Ugeda, M. M. et al. Giant bandgap renormalization and excitonic effects in a monolayer transition metal dichalcogenide semiconductor. *Nat. Mater.* **13**, 1091–1095 (2014).
39. Koperski, M. et al. Optical properties of atomically thin transition metal dichalcogenides: observations and puzzles. *Nanophotonics* **6**, 1289–1308 (2017).
40. Echeverry, J. P., Urbaszek, B., Amand, T., Marie, X. & Gerber, I. C. Splitting between bright and dark excitons in transition metal dichalcogenide monolayers. *Phys. Rev. B* **93**, 121107 (2016).
41. Deilmann, T. & Thygesen, K. S. Dark excitations in monolayer transition metal dichalcogenides. *Phys. Rev. B* **96**, 201113 (2017).
42. Bieniek, M., Szulakowska, L. & Hawrylak, P. Band nesting and exciton spectrum in monolayer  $\text{MoS}_2$ . *Phys. Rev. B* **101**, 125423 (2020).

## Acknowledgements

The work has been supported by EU Graphene Flagship, CNRS via IRP “2D materials”, the ATOMOPTO project (TEAM programme of the Foundation for Polish Science, co-financed by the EU within the ERDFund), the Nano fab facility of the Institut Néel/CNRS/UGA, EMFL, DIR/WK/2018/07 grant from MEiN of Poland and ESF under the project CZ.02.2.69/0.0/0.0/20\_079/0017436. K.W. and T.T. acknowledge support from

the Elemental Strategy Initiative conducted by the MEXT, Japan, (grant no. JPMXP0112101001), JSPS KAKENHI (grant no. JP20H00354), and the CREST (JPMJCR15F3), JST.

## Author contributions

P.K. and M.P. developed the concept and designed the experiment. P.K. performed the experiments with assistance from A.D, D.V. and M.G. P.K., A.O.S. and M.P. interpreted the data. P.K., M.P. and C.F. prepared the manuscript. M.B. prepared the encapsulated sample. K.W. and T.T. produced the hBN crystals. All authors contributed to the discussion of the results and writing the manuscript.

## Competing interests

The authors declare no competing interests.

## Additional information

**Supplementary information** The online version contains supplementary material available at <https://doi.org/10.1038/s42005-021-00692-3>.

**Correspondence** and requests for materials should be addressed to M.P.

**Peer review information** *Communications Physics* thanks the anonymous reviewers for their contribution to the peer review of this work.

**Reprints and permission information** is available at <http://www.nature.com/reprints>

**Publisher's note** Springer Nature remains neutral with regard to jurisdictional claims in published maps and institutional affiliations.



**Open Access** This article is licensed under a Creative Commons Attribution 4.0 International License, which permits use, sharing, adaptation, distribution and reproduction in any medium or format, as long as you give appropriate credit to the original author(s) and the source, provide a link to the Creative Commons license, and indicate if changes were made. The images or other third party material in this article are included in the article's Creative Commons license, unless indicated otherwise in a credit line to the material. If material is not included in the article's Creative Commons license and your intended use is not permitted by statutory regulation or exceeds the permitted use, you will need to obtain permission directly from the copyright holder. To view a copy of this license, visit <http://creativecommons.org/licenses/by/4.0/>.

© The Author(s) 2021